Journal of Bio- and Tribo-Corrosion (2024) 10:17
https://doi.org/10.1007/s40735-023-00816-y

Performance of *Artemisia absinthium* as an Ecological Corrosion Inhibitor in the Industrial Pickling Process

Selma Lamghafri[1] · Walid Daoudi[2] · Abdelmalik El Aatiaoui[2] · Omar Dagdag[3] · Hansang Kim[3] · Fouad Benhiba[4,6] · Avni Berisha[5,7] · Asma Barrahi[6] · W. B. Wan Nik[8] · Abdelkader Zarrouk[6] · Abdellatif Lamhamdi[1]

Received: 1 August 2023 / Revised: 5 December 2023 / Accepted: 30 December 2023 / Published online: 5 February 2024

Abstract

The chemical composition and inhibitory potency of essential oil extracted from the *Artemisia absinthium* plant cultivated in eastern Morocco have been evaluated. The RAO oil constituents were characterized by (GC-MS) and FTIR techniques, the main components were eucalyptol (34.82%), camphor (17.25%), pulegone (12.99%), β-pinene (8.2%), terpene-4-ol (4.2%). The hydro-distilled oil was evaluated as an ecologically corrosion inhibitor while using mild steel (MS) in molar hydrochloric acid. The comportment of the metal in the acidic electrolyte including various concentration of the oil has been examined by the gravimetric method as well as the electrochemical techniques. The inhibitory performance attained 92% at the concentration 2 g/l. Polarization investigation (PDP) demonstrated that the oil was a mixed-type inhibitor and verified Langmuir isotherm model, while the EIS study showed that the corrosion process is controlled by transferring charge. Additionally, the activation and thermodynamic aspects were examined and confirmed the growth of energy barrier and blockage of active site that led to MS corrosion. The steel morphology surface was analyzed using SEM and UV–Vis techniques. Finally, the computed theoretical parameters have been interpreted. These findings provide important information regarding the anticorrosion ability of this essential oil, implying its potential industrial applications.

Selma Lamghafri and Walid Daoudi have contributed equally to this work.

✉ Walid Daoudi
walid.daoudi@ump.ac.ma

✉ Hansang Kim
hskim70@gachon.ac.kr

[1] Laboratory of Applied Sciences, National School of Applied Sciences Al-Hoceima, Abdelmalek Essaadi University, Tetouan, Morocco

[2] Laboratory of Molecular Chemistry, Materials and Environment (LCM2E), Department of Chemistry, Multidisciplinary Faculty of Nador, University Mohamed I, 60700 Nador, Morocco

[3] Department of Mechanical Engineering, Gachon University, Seongnam 13120, Republic of Korea

[4] Laboratory of Advanced Materials and Process Engineering, Faculty of Sciences, Ibn Tofail University, BP 242, 14000 Kenitra, Morocco

[5] Department of Chemistry, Faculty of Natural and Mathematics Science, University of Prishtina, 10000 Prishtina, Kosovo

[6] Laboratoire des Matériaux, Nanotechnologie et Environnement, Faculté des Sciences, Université Mohammed V, Rabat, Maroc

[7] Materials Science-Nanochemistry Research Group, NanoAlb-Unit of Albanian Nanoscience and Nanotechnology, 1000 Tirana, Albania

[8] Faculty of Ocean Engineering Technology and Informatics, Universiti Malaysia Terengganu, 21030, Kuala Nerus, Terengganu, Malaysia

Graphical Abstract

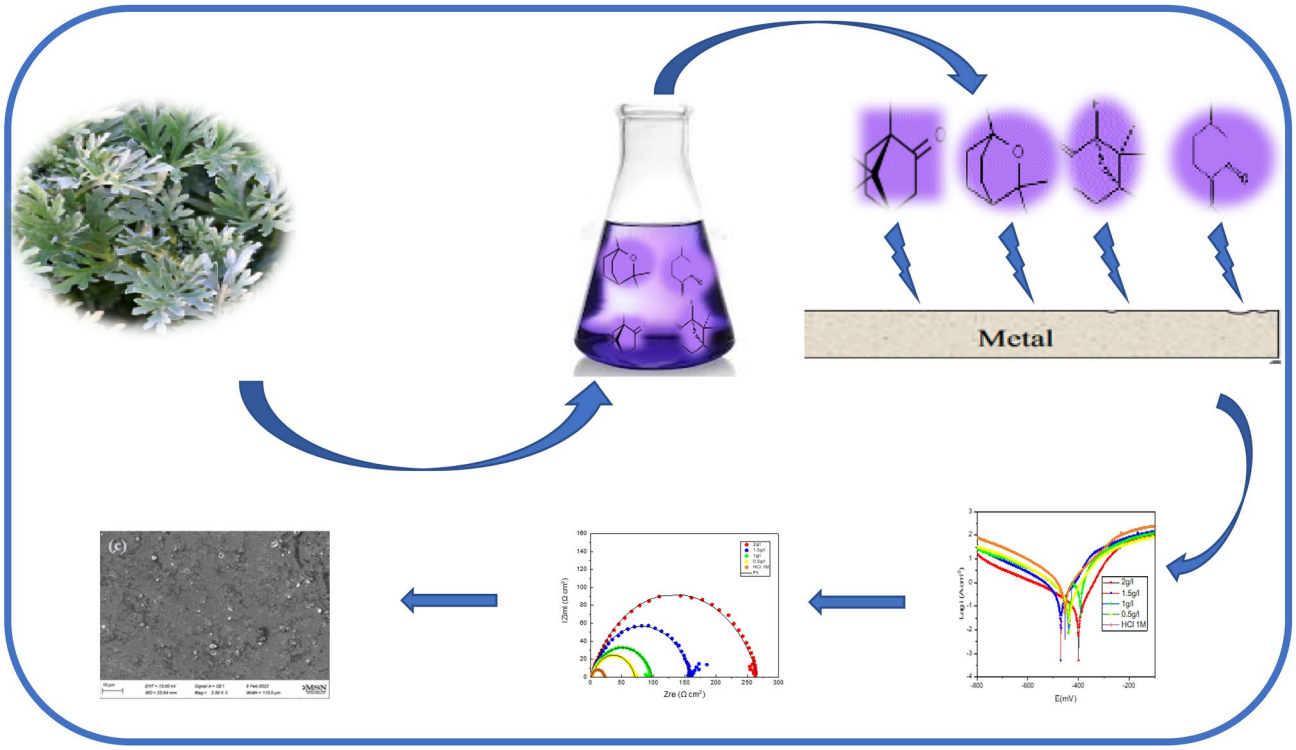

Keywords *Artemisia absinthium* essential oil · Eco-friendly corrosion inhibitor · MS · 1 M HCl · PDP · SEM · Theoretical parameters

1 Introduction

Recently, scientist have given a great interest in the study of the anticorrosive activity of MS in acidic medium owing to its mechanical properties, cheaply priced, elevated accessibility, and strength etc., it is widely applied in different sectors especially industries [1]. The hydrochloric acid is the most used solution in a number of industrial processes, including cleaning, pickling, and acid descaling [2]. However iron and its allows can be easily corroded in these environments, which lead to a great safety and economic damages [3]. With the environmental policies, several methods have been considered to protect MS against corrosion, the use of safe, effective and environmental friendly inhibitors is among the most effective methods for preventing rust even at low concentrations [4], they act by adsorption into the substrate surface and establish a barrier toward corrosive substances [5], according to the literature an effective organic inhibitor should be chemisorbed on the substrate surface with a high adsorption energy and form a compact barrier layer with an inner thickness very high [6]. Heteroatoms, namely oxygen, nitrogen, phosphorus, or sulfur, and the unsaturated bonding provide the non-bonded electrons which are necessary for the adhesion process of the organic compound on the substrate surface [7–9]. However, few of the synthetic inhibitors are safe, although most of them are extremely toxic, expensive [10], and non-biodegradable that is why recently researchers are focused on eco-friendly environment inhibitors [11]. Natural plants, extracts, oil or pure compounds, that presents better anticorrosive features, prevents pollution, keeps the environment secure, and healthy [12]. Because they are safe for the environment, renewable and affordable [13, 14], oils derived from various plants are employed as inhibitors of corrosion and have been stated by numerous authors. Jojoba oil has been examined on iron in 1 M HCl by Chetouani et al. [15], at a concentration of around 0.51 g/l, it exhibits good inhibitory efficacy of almost 100% and follows Frumkin adsorption Rosemary oil has been investigated by Chaieb et al. [16] on H_2PO_4, at an amount of 16 g/l, the inhibitor attained an inhibiting potency of about 73%. El Aatiaoui et al. [17] studied the anti-corrosive properties of *Calamintha* plant leaf oil in 1 M HCl for MS, they reported that the maximum efficiency attaint was 87.57% observed for 1.5 g/l of EOC. Bouyanzer et al. [18] studied the *oil of Pennyroyal* obtained from *Mentha pulegium* for steel in 1 M HCl they

found out that this oil exhibited good anticorrosion properties and attained maximum value of inhibition efficiency at 2.76 g/l, the oil affected the cathodic hydrogen reduction and acted as cathodic inhibitor. Kurniawan et al. [19], studied *capsicol oil* of red *pepper seed* on stainless steel in acidic electrolyte, the oil is potent in the inhibition of corrosion process, its inhibition efficacy reached 92.32% and decreased with temperature. Loto [20] investigated Low carbon steel's corrosion-inhibiting characteristics (LCS) in 0.5 M H_2SO_4 and HCl of two inhibitors, *extracts of basil CLB and atlas cedar* CLA *oils* admixed separately with clove essential oil extracts the results showed high inhibitory efficiency 95.48% and 95.32% in H_2SO_4 and 92.7% and 97.98% for CLB and CLA, respectively.

This research aims to assess the anticorrosive effect of *Artemisia absinthium* essential oil (RAO) on metals in a 1 M HCl environment. *A. absinthium*, also known as absinthe, originally belongs to the Asteraceae family [21]. Harvested from a semi-arid region in Morocco, it finds widespread use in the pharmaceutical sector and for therapeutic applications. The novelty of this study lies in defining the chemical composition of this plant, cultivated in the Driouch region in eastern Morocco, and presenting the current state of knowledge regarding the potent capability of this oil in inhibiting mild steel (MS) corrosion. Furthermore, the essential oil was extracted using a simple hydrodistillation method with water as the solvent. For this purpose, GC-MS and FTIR methods were used to identify the main components of the extracted oil. Also, we have used specifically, electrochemical approaches PDP and EIS as well as the gravimetric method to understand the process of the inhibitor's interaction with the metal surface, also to identify active spots in the adsorption procedure. The MS's surface has been analyzed using SEM analysis, the UV has been utilized in order to confirm the complex formation. finally, a quantum study has been carried out for the purpose of extending the experimental investigations and to elaborate the relationship between this latter and quantum calculations, for this purpose, several quantum techniques have been performed to relate the molecular features of the organic inhibitor with the inhibitory efficiency IE (%).

2 Experimental

2.1 Extraction of Essential Oil

Artemisia absinthium's essential oil RAO was extracted from the leaves part collected from the east of Morocco with a 3.3 average yield. We have utilized the hydro-distillation method, in a 1 l round bottom container with around 500 ml of water, we have added 5 g of *A. absinthium* plant leaves and brought to a boil, the steam was directed to a condenser column. Finally, the oil RAO was removed due to the difference in density. The obtained volatile oil was purple having aromatic scents and agreeable fragrance.

2.2 GC-MS and FT-IR Investigation

In order to recognize different functional groups existing in the RAO oil, GC-MS technique has been utilized, also FTIR method was used to furnish further qualitative data needed to identify elements.

2.3 Mild Steel and Electrolyte

The steel electrodes are composed of the following chemical elements 99.25% iron, 0.21% carbon, 0.1% manganese, 0.35% phosphorus, 0.05% sulfur, and 0.04% aluminum were handily abraded using silicon carbide papers it goes from 200 and ended 2000 grit size, after that the MS went through distilled water washing, acetone degreasing, and air drying, just after it has been embedded into the cell and leaving a 1 cm^2 surface exposed, the electrical contact for the electrochemical investigation was assured by copper wires. The corrosive medium (1 M HCl) was prepared from the analytic content consisting of pure water and 37% HCl.

2.4 Weight Loss Study

Right after been washed, MS specimens were plunged into 1 M HCl medium for 6 h at temperature of 303 K with and without different concentration of inhibitors. After that, using distilled water, the samples were thoroughly cleaned, and dried then weighed with high precision. The rate of corrosion ω_{corr} was calculated using the mean of triplicate experiences using the Eq. (1) and the inhibition efficacy $\eta_w(\%)$ is determined basing to the formulas (2) [22]:

$$W_{corr} = \frac{m_i - m_f}{S \times t} \tag{1}$$

$$\eta_w = \left(1 - \frac{W_{corr/inh}}{W_{corr}}\right) \times 100 \tag{2}$$

2.5 Electrochemical Study

The electrochemical tests have been evaluated in a solution containing several amounts of RAO oil (2 g/l–0.5 g/l). For the tests, we have used a cell with three electrodes consisting of working electrode (WE) which is MS, a saturated calomel electrode (SCE) was employed as the reference electrode (RE), with a Pt electrode serving as the counter electrode (CE), these latter are associated to PGZ 402 potentiostat/galvanostat. The polarization data were registered after 30 min

to reach the stable potential OCP and using 0.5 mV/s of scan speed in the range (− 800 to 0 mV). The inhibitory effectiveness η_{PDP} (%) is generated from the relation bellow [23]:

$$\eta_{PDP} = \left(1 - \frac{i^0_{corr}}{i_{corr}}\right) \times 100, \quad (3)$$

where i^0_{corr} is the blank current density while i_{corr} stands for the studied inhibitors current density. While, the EIS measurements were obtained in the frequency range between 100 kHz and 10 mHz that has a perturbation of 10 mV, the outcome is then affined with Z-View Software. The inhibition efficiencies (η_{EIS}(%)) have been calculated using the following expression [24]:

$$\eta_{EIS} = \left(1 - \frac{R^0_p}{R_p}\right) \times 100, \quad (4)$$

where R_p and $R_p{}^0$ symbolize the polarization resistance with and without inhibitors, respectively.

2.6 SEM and UV–Vis Investigation

With the objective to observe the surface morphological changes of the carbon steel, this latter has been dipped in the inhibited solution and then has been examined by SEM analysis. To further analyzed the MS surface, UV–Vis analysis has demonstrated that a complex has formed between ferrous and the MS surface, utilizing a Jasco V-730 spectrophotometer after a 24-h immersion of the MS in the inhibited and uninhibited electrolyte.

2.7 Theoretical Investigations

The geometry optimisation was performed with the Gaussian 16 program package, based on the DFT method, using the functions 6-311+g(d,p)/apfd/smd (water) model [25].

To study and understand interactions between the β-pinene, camphor, eucalyptol, terpene-4-ol, and pulegone molecules with the MS interface, this latter was conducted using MC and MD simulations. These simulations are widely used to determine the different adsorption configurations and the interaction system between the molecular structure of the β-pinene, camphor, eucalyptol, terpene-4-ol, and pulegone molecules and the MS surface. Materials Studio 8.0 software was used to perform the MC and MD simulations [26–31].

3 Findings and Discussion

3.1 *Artemisia absinthium* Oil Composition

The GC-MS chromatographic spectrum of RAO essential oil allows the determination of different present elements. The examined oil reveals the presence of a combination of compounds involving about twenty various species, the main constitutes are eucalyptol, camphor, pulegone, β-pinene, terpene-4-ol, as illustrated in Fig. 1.

The east Morocco RAO oil compositions are considerably different from those retrieved in Tajikistan, Middle East, Europe, Asia, each regions represents new phytochemicals [32]. Table 1 regroups the compounds constituting the oil.

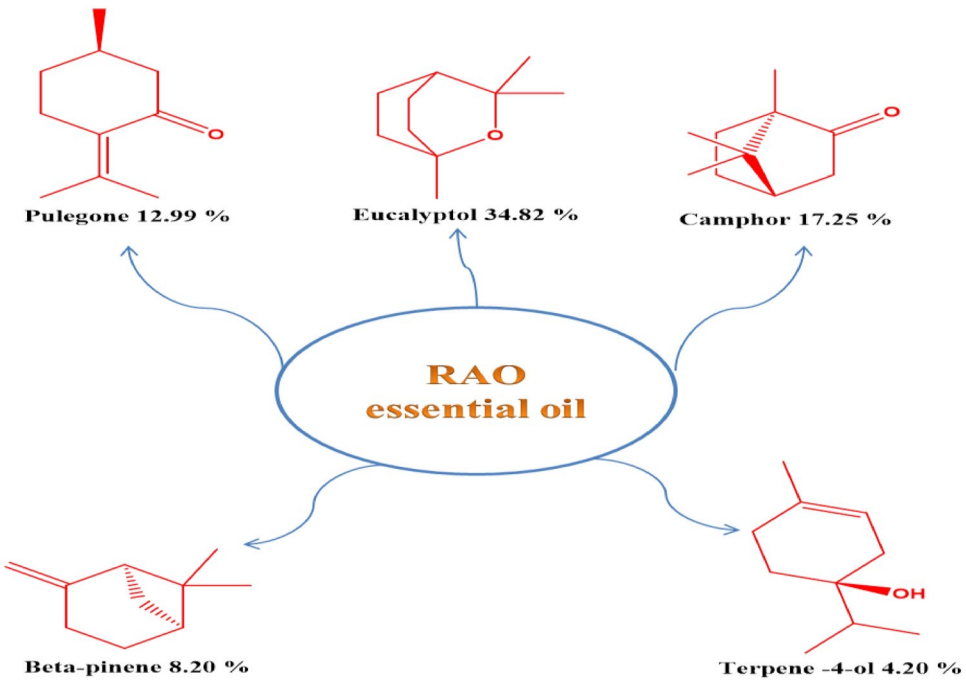

Fig. 1 Main constituents of *A. absinthium*

Table 1 Various compounds constituting RAO oil

No.	Nom	Tr	% Air
1	Alpha.-Pinene	5.195	3.44
2	Camphene	5.457	1.28
3	Beta.-Pinene	5.926	8.20
4	Beta.-Myrcene	6.098	2.72
5	2-Carene	6.572	0.54
6	m-Cymene	6.727	1.02
7	Eucalyptol	6.842	34.82
8	Gamma.-Terpinene	7.277	1.24
9	L-Fenchone	7.814	0.74
10	Beta.-Linalool	7.986	4.18
11	Camphor	8.787	17.25
12	Pinocarvone	9.066	0.52
13	*p*-Menth-1-en-8-ol	9.178	0.61
14	Terpene-4-ol	9.324	4.20
15	Alpha.-Terpineol	9.558	0.78
16	1R)-(−)-Myrtenal	9.605	1.59
17	Pulegone	10.275	12.99
18	Eudesma-4(14),11-diene	13.899	0.91
19	Alpha.-Bisabolene	14.465	0.85
20	Chamazulen	17.076	2.12

In addition, the RAO oil was evaluated by FT-IR techniques to know the existent functional groups the RAO bioactive. Figure 2 represents the spectrogram of the RAO oil.

According to the spectrogram of RAO, a broad band is present at 3400 cm^{-1}, which was a result of the vibration of the OH group, that confirms the presence of Eucalyptol in RAO. In addition, bands were recorded at 2922 cm^{-1} and 2852 cm^{-1} indicating C–H vibrations which are symmetric and asymmetric, respectively. Also, the aromatic C=O vibration is responsible for a band at 1723 cm^{-1}, therefore the presence of pulegone in RAO. On the other hand, at 1455 cm^{-1}, a CH bending vibration was detected, moreover, the bands associated with wave numbers 1272 cm^{-1}, 1100 cm^{-1} are attributed to CC and CO vibrations, respectively.

3.2 Open Circuit Potential Analysis

It can be noticed from Fig. 3 that the open circuit potential (OCP) of steel in 1 M HCl preceding and following the addition of several amounts of oil. It is clear from the OCP curve that the E_{corr} values in the blank solution are anodically shifted until they reach the equilibrium state. This can be considered as the initial layer of the oxide coating generated by air on MS. In addition, it could be noticed that the carbon steel E_{corr} value was observed in the more positive zone at the highest concentration of 2 g/l, indicating that the oil adheres to the steel surface and has a significantly higher inhibitory influence on the anodic reaction than its impact on the cathodic reaction. Furthermore, with the addition of different amounts of RAO, the E_{corr} shifted toward negative potentials with respect to the blank, which can be interpreted as the resultant effect on the cathodic corrosion reaction.

3.3 Potentiodynamic Polarization (PDP)

Data resulting from PDP experiment for the MS in the 1 M HCl at varying inhibitor doses are observed in Fig. 4.

According to the plot we can clearly see that after addition of the inhibitor the curves have minor changes in comparison with the blank solution. In another term, both the anodic and cathodic reactions are impacted by the introduction of inhibitors to the solution [33]. The PDP parameters are summarized in Table 2.

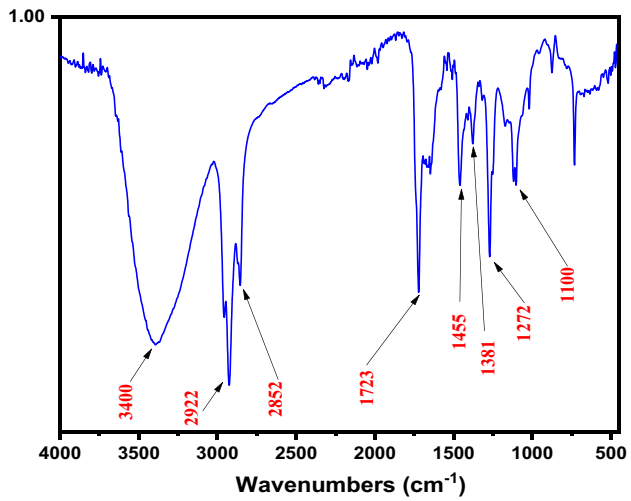

Fig. 2 FT-IR spectrogram of RAO oil

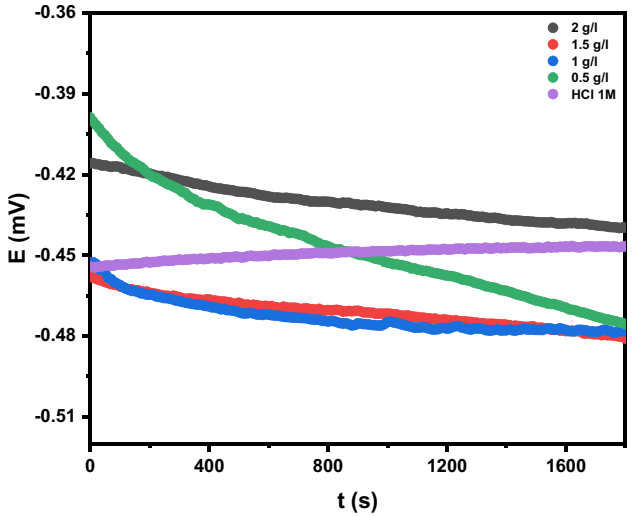

Fig. 3 Open circuit potential curves

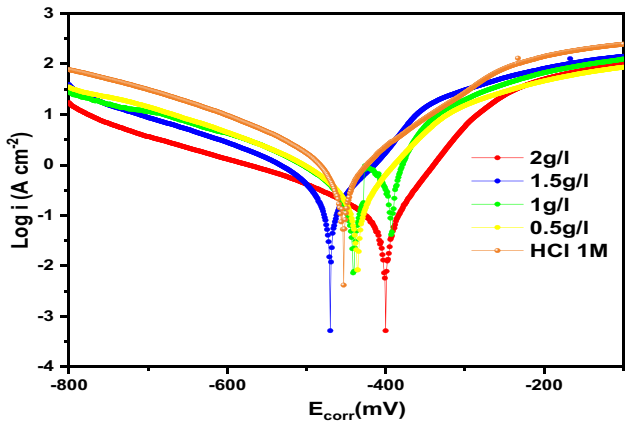

Fig. 4 Tafel's curves for different concentrations of the RAO oil

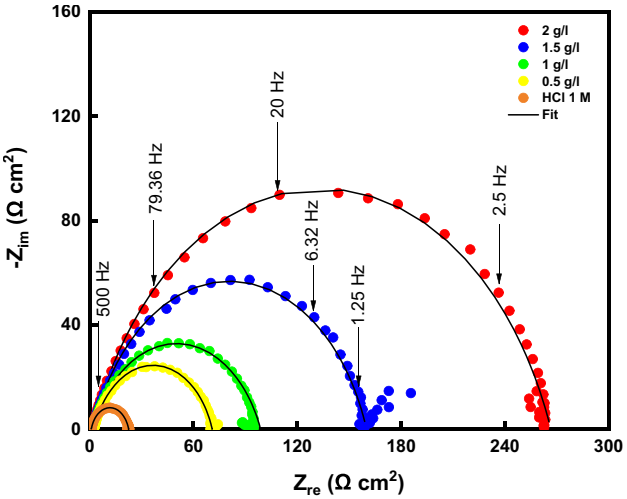

Fig. 5 Nyquist diagrams for the MS at different concentrations of RAO oil in 1 M HCl

From Table 2, we can notice that the deviation between the E_{corr} in the inhibited solution and the E_{corr} for the uninhibited one remains inferior to 85 mV, according to the literature this inhibitor belongs to the class of mixed-type inhibitor [34]. It can also be noted that the i_{corr} is decreasing with the addition of the oil, it goes from 1104.3 to 81.7 µA/cm^2 at 2 g/l, possibly caused by the adsorption of phytochemicals present in *A. absinthium* [35], indicating the inhibitors efficiency which attained 92.60% at the optimum concentration. We can also notice a large linearity in the cathodic part proving that Tafel law is validated and the discharge of the H^+ proton is accomplished in accordance with pure activation kinetics [36], it is also noted a variation in the value of both cathodic and anodic slopes of Tafel indicating that the hydrogen evolution affects the cathodic reaction and the anodic reaction is impacted by the MS dissolving [37].

3.4 EIS Measurements

EIS has proved to be an effective method to comprehend the inhibitor adsorption occurring at the substrate interface in an acidic medium and to evaluate the electrochemical behavior while including different amounts of the oil [38]. Figures 5 and 6 display the Bode and phase representations as well as the Nyquist graphs for the steel in 1 M HCl.

According to Nyquist plots capacitive loops are observed, indicating the presence of double layer capacitance and that charge-transfer controls the corrosion process [39], the size of these depressed semi-circles, rises with the inclusion of *A. absinthium* which might be related to the effectiveness of the oil in mitigating the steel corrosion [40], and the non-ideal comportment is probably caused by the frequency dispersion brought on by the inhomogeneity of the MS surface [41]. Figure 6 shows that at low frequencies the absolute modulus impedance |Z| is steadily increasing by addition of essential oil RAO indicating that MS is covered by organic molecules after being adsorbed [42]. The lone peak noted in the plots of Bode reveals the existence of a single time constant [43]. Phase angles values increase with the addition of inhibitor indicating better coverage of the MS surface [44], however their values remind inferior to 90° confirming the non-ideal behavior of the system [45]. The EIS parameters were evaluated using the slightest square adjustment of the equivalent circuit; the results are displayed in Table 3.

From the table, we can notice an increase in R_p values and a diminishing in capacitance with the increase of the organic molecule concentration explained by a thickening of the double layer and/or a decreasing in the dielectric constant [46], this is interpretable by the impede of transfer of charges and development of a barrier resulting from oil adsorption on the steel surface [47]. Additionally, the

Table 2 PDP parameters for different RAO concentrations

Comp.	C_{inh} (g/l)	$-E_{corr}$ (mV/ECS)	i_{corr} (µA/cm^2)	$-\beta_c$ (mV/dec)	β_a (mV/dec)	η_{PDP} (%)
Blank	0	456.3	1104.3 ± 0.2	112.8	155.4	–
RAO oil	2	399.213	81.706 ± 0.1	142.7	54.4	92.60
	1.5	469.015	131.647 ± 0.2	65.4	61.8	88.07
	1 g	440.097	205.371 ± 0.2	96.5	87.0	81.40
	0.5	435.078	299.653 ± 0.4	130.4	73.4	72.86

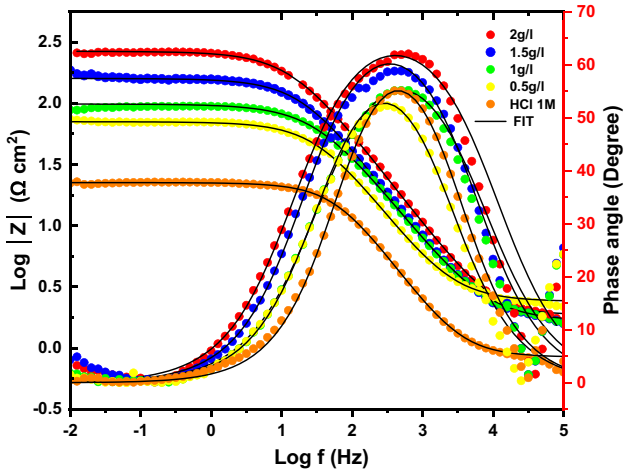

Fig. 6 Plots of Bode and phase for MS at various RAO oil concentrations in the 1 M HCl

n values provide details concerning the state of the surface heterogeneity. When n is close to 1, the CPE can be considered as a perfect, polished-surface capacitor; however, when n is zero, the CPE can act like a resistor. If n is between 0 and 1, it represents intermediate behavior between a capacitor and a resistor [48], In our case n values are between 0 and 1, which indicate a typical ideal CPE constant, these values are inferior than that of the blank (0.841) indicating the existence of a thin layer that was generated on the surface of the steel [49]. Moreover, R_s values are more pronounced in all concentrations of the inhibited solution compared to that in the hydrochloric acid medium it goes from 0.84135 Ω cm^2 at 2 g/l to 1.553 Ω cm^2 for the blank indicating that between the steel surface and the electrolyte, the transfer of charge is more activated. The inhibitory effectiveness of the oil RAO to protect MS reached 91.85%, this could be related to the synergic effect of the RAO oil phytochemicals [50]. Additionally, the chi-squared values χ^2 are used to determine the appropriateness of fit, the great fitting quality of the data is accomplished by using appropriately low chi-square values. As it is reported from Table 3 the obtained chi-square values are of the order of 10^{-3} indicating that the fitting error is relatively low and that the model utilized is very accurate proving high agreement between the experimental data and the fitted values. The impedance findings were adjusted using the following equivalent electrical circuit (EEC) (Fig. 7).

3.5 Gravimetric Measurements

Weight loss tests were evaluated for the steel substrate in HCl 1 M in presence and without different amounts of the *A. absinthium* oil RAO ranging from 2 to 0.5 g/l, the resulting is grouped in Table 4.

According to Table 4 It is evident that adding oil to an acidic solution lowers the rate of corrosion from 0.4325 mg/cm^2/h for the uninhibited medium to 0.0357 mg/cm^2/h for the inhibited one, in deed the η_w (%) rises with the increase of the oil amounts added to the aggressive solution, it reached 91.63% at the optimum concentration 2 g/l of *A. absinthium* oil. This outcome is explicable by the increase of the surface covered by a thin protective barrier of the phytochemicals of the essential oil formed at the MS interface [51]. The findings are closely correlated with the ones obtained by the PDP and EIS techniques. Figure 8 compares the inhibition efficacy attained by the three methods.

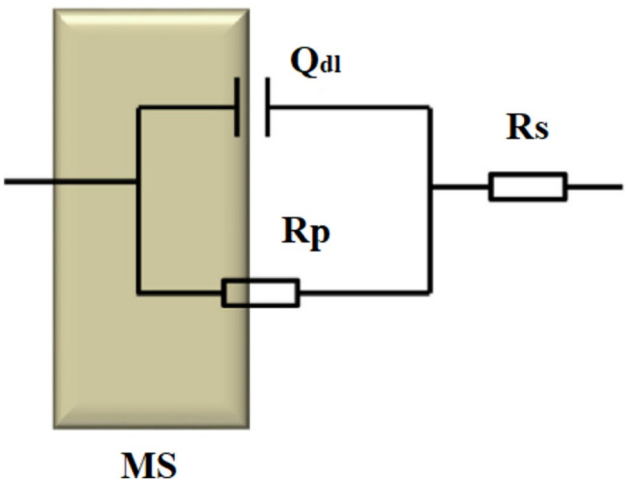

Fig. 7 EEC describing the studied system

Table 3 EIS data at various concentrations of RAO oil for MS in 1 M HCl

Comp	C_{inh} (g/l)	R_s (Ω cm^2)	R_p (Ω cm^2)	C_{dl} (μF/cm^2)	Q_{dl} (μF s^{n-1}/cm^2)	n_{dl}	η_{EIS} (%)	$\chi^2 \times 10^{-3}$
HCl	–	0.841 ± 0.006	21.61 ± 0.01	120.4	309.38 ± 0.01	0.841 ± 0.005	–	2.2
RAO oil	2	1.553 ± 0.035	265.11 ± 0.01	40.7	113.04 ± 0.01	0.774 ± 0.003	91.85	1.92
	1.5	1.844 ± 0.015	158.21 ± 0.01	48.8	133.60 ± 0.01	0.793 ± 0.004	86.34	4.8
	1	1.656 ± 0.025	97.18 ± 0.01	49.0	178.36 ± 0.01	0.758 ± 0.002	77.77	0.07
	0.5	2.398 ± 0.007	68.44 ± 0.01	68.5	206.80 ± 0.02	0.794 ± 0.002	68.42	1.89

Table 4 Gravimetric data for the studied system

Comp.	Conc.	Corrosion rate (mg/cm^2/h)				η_w (%)
		1st test	2nd test	3nd test	Mean	
Blank	1 M	0.4516	0.4213	0.4325	0.43513 ± 0.01	–
RAO oil	2 g/l	0.0355	0.0381	0.0357	0.03643 ± 0.001	91.63
	1.5 g/l	0.0560	0.0502	0.0551	0.05377 ± 0.003	87.65
	1 g/l	0.0838	0.0867	0.0887	0.0864 ± 0.002	80.62
	0.5 g/l	0.0923	0.0995	0.1304	0.1074 ± 0.02	75.31

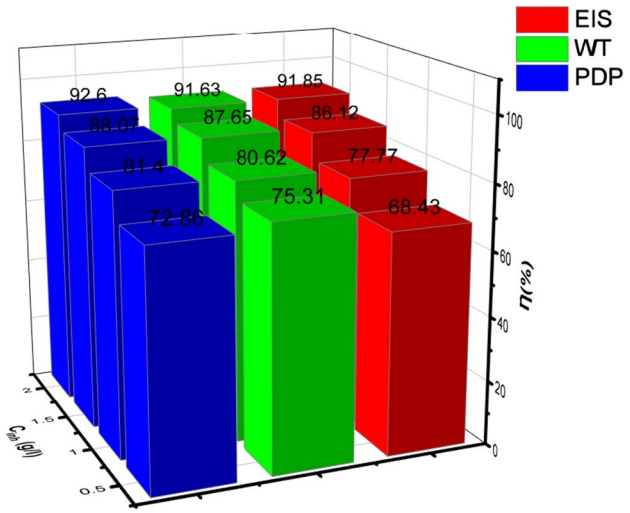

Fig. 8 Inhibitory efficiencies obtained from different techniques

3.6 Immersion Time Effect

The Immersion time effect was examined by the loss weight method for MS in HCl medium at a temperature equal to 303K for different concentration of the oil within the range of 3 to 7 h. Table 5 summarizes the results obtained, also plots of the η_w(%) of the natural oil versus various concentration are represented in Fig. 9.

From Table 5, We can easily observe that as concentration and time rise, the η(%) increases, for the optimal amount of 2 g/l the inhibiting power varies between 38.24% for 3 h and 91.63% for 6 h, this indicates a progressive creation of a barrier layer over the substrate's surface [12]. However, above the six hours of the study period, the inhibitory effectiveness begins to diminish, according to the literature some authors have explained this decrease after a long immersion period by the exhaustion of the available inhibitor molecules in solution [52], this can be attributed to a formation of chelate between iron and organic phytochemicals [53]. These findings allow us to assess the effectiveness and the anticorrosion performance of *A. absinthium* essential oil RAO.

3.7 Temperature Effect

Generally, temperature effect investigates the impact of temperature on the rate of corrosion and dissolution of the metal [54]. The temperature effect on the η_{PDP} (%) of the MS in existence and absence of different amount of the RAO oil was investigated by employing PDP technique in the temperature range of 303-333K. The polarization curves are shown in Fig. 10, and the PDP data are regrouped in Table 6.

In the absence of *A. absinthium* oil, it is obvious that a rise in temperature causes an increase in i_{corr} indicating the impact of corrosive agents on the substrate [55]. However, the addition of the oil RAO to the acidic medium results in a diminishing of i_{corr} values this is due to the inhibitory proprieties of the oil at the temperature range [56]. It is also noticed that the η_{PDP} (%) decreases steadily with augmenting temperature, it goes from 92.60% to 89.40% suggesting that the organic molecules have been desorbed from the MS surface. However, the η_{PDP} (%) remains higher than 89% indicating the oil effectiveness is potent even in high temperature.

Table 5 Inhibitory efficiency at different immersion time of the RAO oil

Comp.	Conc.	η_w (%)				
		3 h	4 h	5 h	6 h	7 h
Blank	1 M	–	–	–	–	–
RAO oil	2 g/l	38.24	50.35	69.32	91.63	83.78
	1.5 g/l	24.24	32.11	50.83	87.65	73.83
	1 g/l	14.33	23.24	35.76	80.62	71.76
	0.5 g/l	7.45	8.56	17.39	75.31	67.53

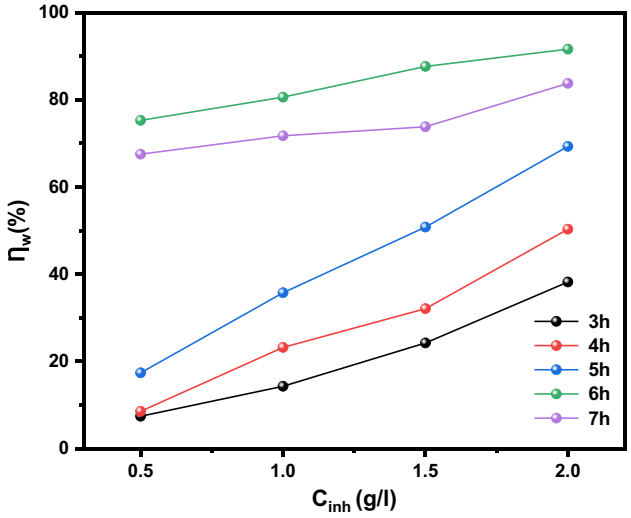

Fig. 9 Inhibition efficiencies for various concentrations of RAO oil at different immersion time

3.8 Thermodynamic Activation Parameters

In the aim to calculate kinetic parameters for the corroding procedure namely the energy of activation (E_a), the enthalpy and the entropy ΔH_a and ΔS_a, respectively, results obtained from the temperature effect investigation enabled us to represent $\ln(i_{corr}/T)$ as well as $\ln(i_{corr})$ as a function of $10^3/T$ (Fig. 11).

We have obtained quiet Straight lines, from which we have applied Arrhenius equation and Arrhenius transition state for calculating the activation parameters:

$$\ln\left(i_{corr}\right) = \ln(A) - \frac{E_a}{RT} \tag{5}$$

$$\ln\left(\frac{i_{corr}}{T}\right) = \left[\ln\left(\frac{R}{Nh}\right) + \left(\frac{\Delta S_a}{R}\right)\right] - \frac{\Delta H_a}{RT} \tag{6}$$

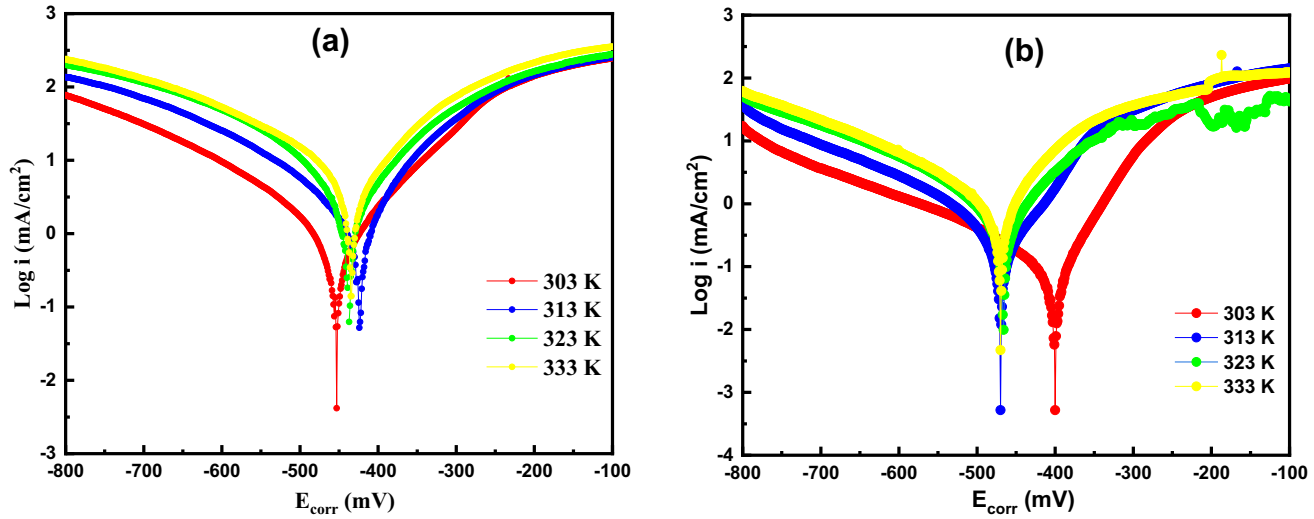

Fig. 10 PDP polarization curves of MS at different uninhibited (**a**) and RAO-inhibited (**b**) solution temperatures

Table 6 PDP parameters for MS with and without RAO oil

Comp.	Temp. (K)	$-E_{corr}$ (Mv vs CSE)	i_{corr} (μA/cm^2)	$-\beta_c$ (mV)	β_a (mV)	η_{PDP} (%)
Blank	303	456.3	1104.3 ± 0.4	112.8	155.4	–
	313	423.5	1477.4 ± 0.01	131.3	91.3	–
	323	436.3	2254 ± 0.02	117.8	91.4	–
	333	433.3	3944.9 ± 0.04	134.6	103.9	–
RAO oil	303	399.2	81.7 ± 0.001	142.7	54.4	92.60
	313	470.4	118.9 ± 0.2	58.8	59.9	91.94
	323	466.4	209.1 ± 0.3	54.0	45.0	90.72
	333	469.4	418.0 ± 0.5	75.4	48.8	89.40

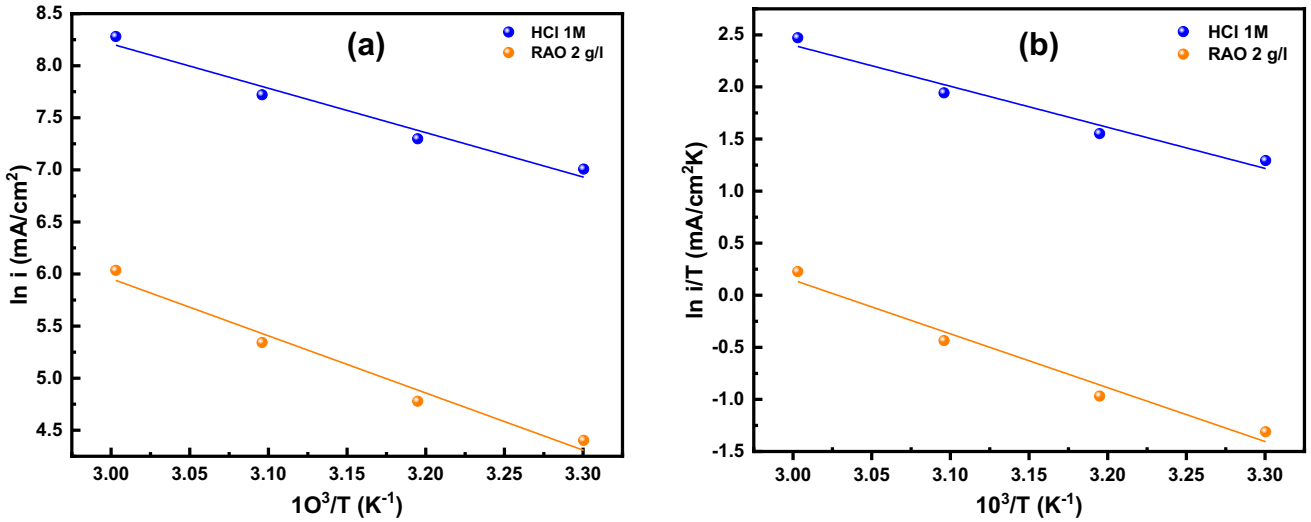

Fig. 11 Arrhenius lines (**a**) and Arrhenius transition lines (**b**) of the studied system

E_a/R represents the line slope derived from $\ln(i_{corr})$ vs $10^3/T$, $\Delta H_a/R$ and $(\Delta S_a/R + \ln R/Nh)$ are the slope and the intersection of $\ln(i_{corr}/T)$ vs $10^3/T$, respectively. The calculated thermodynamic parameters are presented in Table 7.

It is obvious that in presence of the *A. absinthium* oil, E_a of the solution including oil is greater than that of the blank, that is generally attributed to energy barrier growth and active site blockage leading to MS corrosion [57]. The endothermic aspect of the rust process is explained by the positive value of the ΔH_a, while the negative value of the ΔS_a indicates the electrolyte's disorder diminishing [58], this is interpreted by the exhaustion of the organic molecules existing in the solution by their association with iron atoms on the MS surface through adsorption process [59].

3.9 SEM Investigation

To closely visualize MS's morphology and surface, SEM technique have been used. Figure 12a shows the abraded steel surface with few scratches, Fig. 12b demonstrates an extensively damaged surface for the steel emerged in HCl medium without essential oil, however after the inclusion of the RAO oil we can see in Fig. 12c a neat and uniform surface, this finding confirms the fact of existence of a thin layer covering the metal surface and shielding it from damaging ions [60].

Table 7 Thermodynamic data for the evaluated system

Comp.	R^2	E_a (kJ/mol)	ΔH_a (kJ/mol)	ΔS_a (J/mol K)	$E_a - \Delta H_a$ (kJ/mol)
Blanc	0.9717	35.42	32.78	− 79.2	2.64
RAO oil	0.9753	45.62	42.98	− 67.37	2.64

3.10 UV–Vis Analysis

To further analyze the carbon steel surface and to confirm the development of a complex between ferrous and the MS surface, the UV–Vis analysis has been performed. In this context, we have registered the UV–Vis spectrum of the molar hydrochloric medium including 2 g/l of RAO before and after immersion of the substrate for 24 h, the results are plotted in Fig. 13.

In general, the change in absorbance value and/or shifting of the wavelength suggest that a complex has formed between the two chemicals in solution. According to the plots, we can clearly notice two wavelength bands at 286 nm and 241 nm before immersion. However, after 24 h of dipping, the intensity levels of these wavelength bands decreased from the previous ones, as depicted in Fig. 13. The observed shift in the spectra of the solution ahead of immersion and after submerged of steel is explained by metal–inhibitor interactions and development of complexes involving iron and inhibitors molecules in 1 M HCl.

3.11 Theoretical Conception

3.11.1 DFT Results

The reactivity of the inhibitor is strongly correlated with its adhesion on the MS interface via donor–acceptor interactions [61, 62]. Based on Fukui's hypothesis, it is possible to predict the manner that the inhibitor will react with the metallic surface using the molecular orbital frontiers HOMO

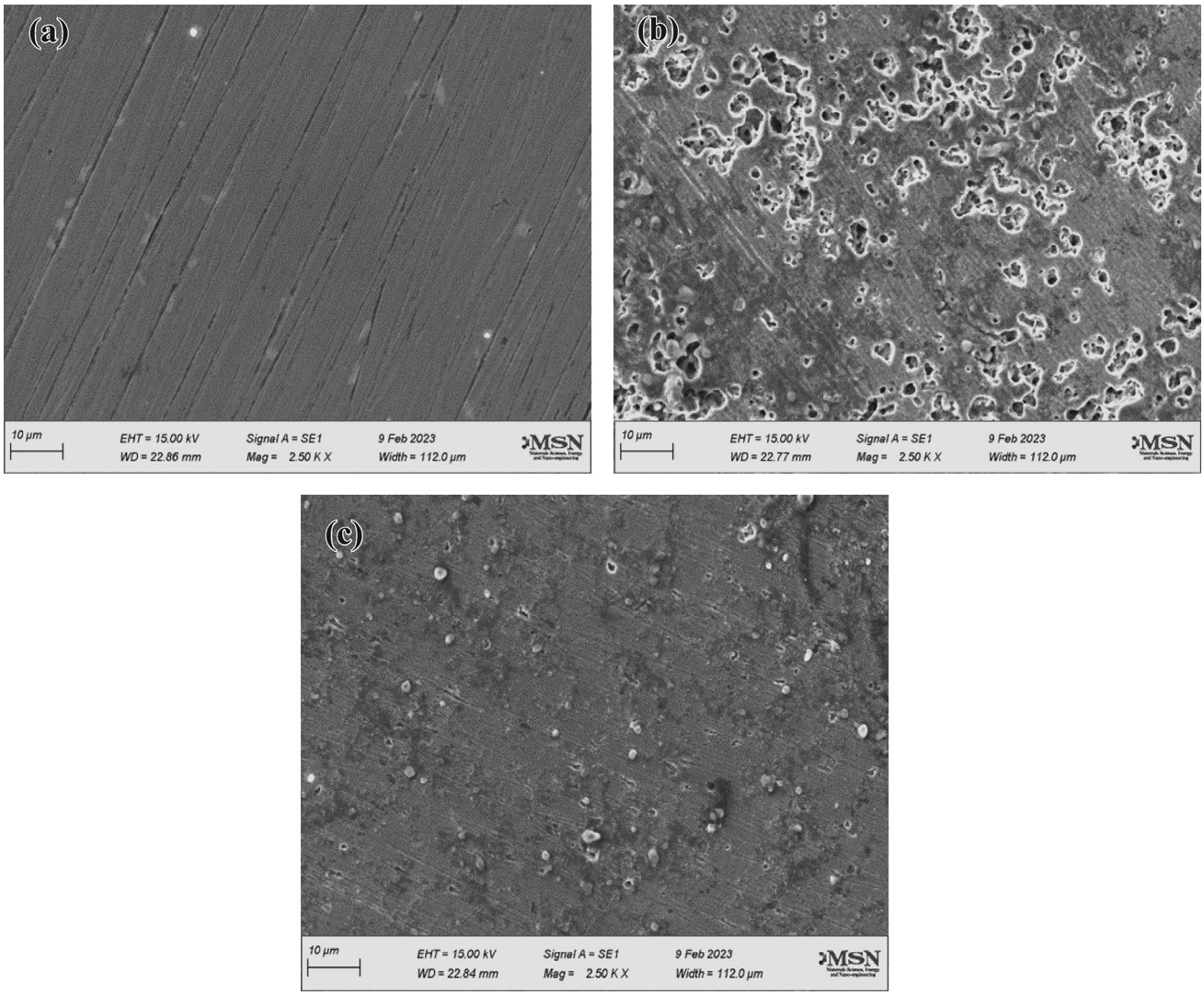

Fig. 12 SEM pictures of MS (**a**) in the absence (**b**) and presence (**c**) of RAO in 1 M HCl

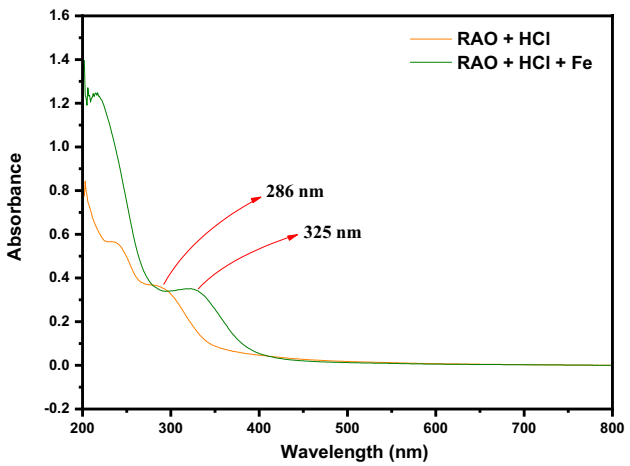

Fig. 13 UV–Vis spectrograph of RAO-inhibited acid solution before and after metal immersion

and LUMO. HOMO is the orbital which might act like an electron donor, and the electron donor capacity increases as its E_{HOMO} energy increases [63]. Conversely, LUMO is the orbital capable of accepting electrons, and the inhibitor ability to accept electrons from metal atoms is increased by a lower E_{LUMO} value [64].

The electron density distributions of the frontier orbitals are of great significance in fully explaining the inhibitors adsorption preference [65]. HOMO and LUMO orbital electron density distributions of the five chosen inhibitors are illustrated in Fig. 14.

For understanding electrophilic engraving spots and nucleophilic reactions, molecular electrostatic potential (ESP) is connected to electrical density and is an extremely valuable descriptor [66]. The primary compounds found in RAO oil are shown in Fig. 14 by their ESPs. Positive (blue) and negative (red) sections of the ESP are correlated with nucleophilic and

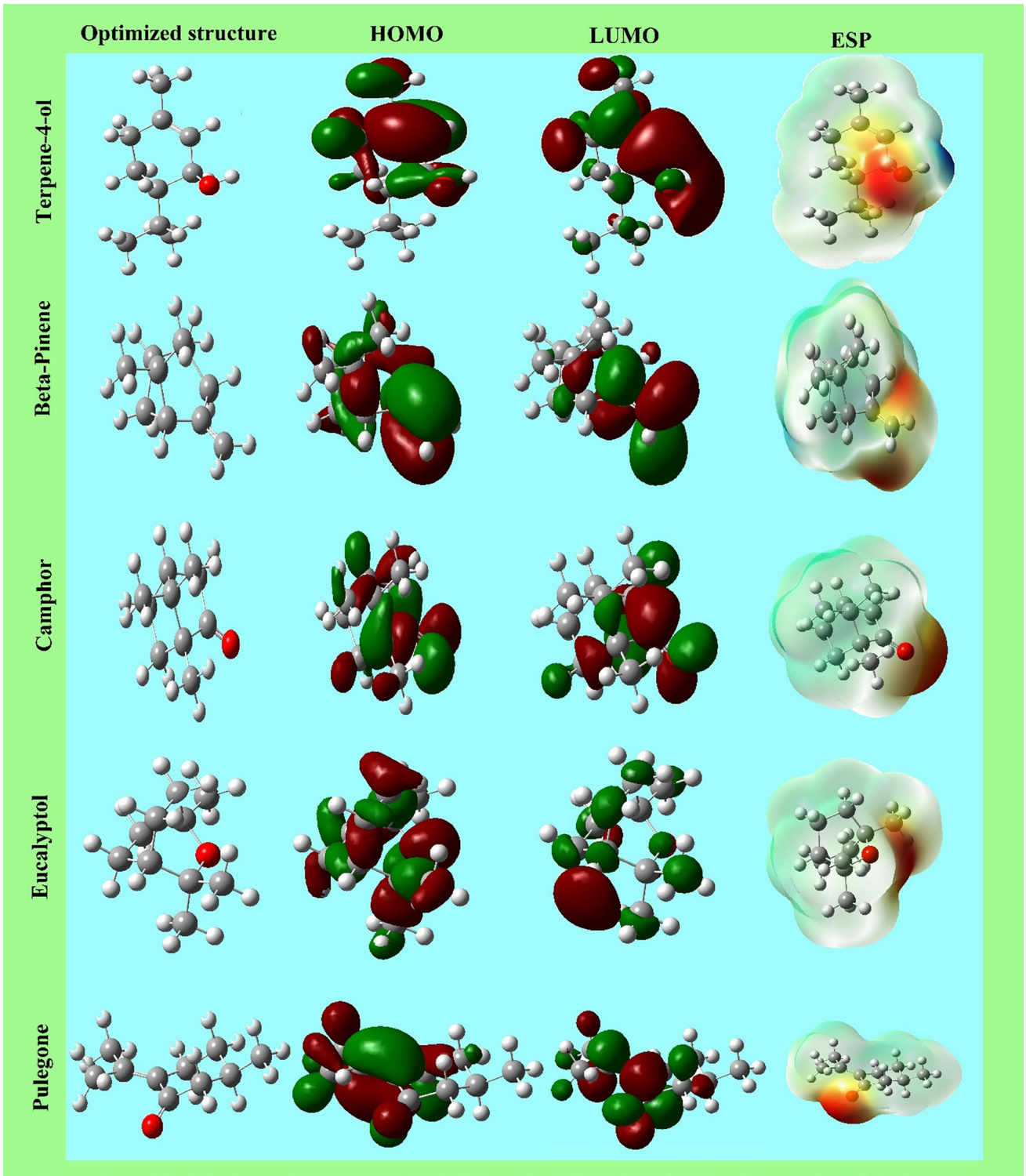

Fig. 14 Optimized structure, HOMO, LUMO, and ESP pictures of β-pinene, camphor, eucalyptol, terpene-4-ol, and pulegone molecules (Color figure online)

electrophilic reactivity, respectively [67]. It is apparent that the areas richer in electrons are primarily around oxygen atoms and conjugated double bonds. As a consequence, MS functions as an electrophile which is able to attract nucleophilic centers (heteroatoms with free electron pairs) from inhibitory molecules.

Table 8 Quantum functions for the essential molecules of RAO molecules

Theoretical parameters	Terpene-4-ol	β-pinene	Camphor	Eucalyptol	Pulegone
E_{HOMO} (eV)	− 6.6767	− 6.6388	− 6.9775	− 6.8164	− 6.7786
E_{LUMO} (eV)	0.255	0.221	− 0.6559	0.4345	− 1.2483
ΔE (E_{HOMO}–E_{LUMO}) (eV)	6.9316	6.8599	6.3216	7.251	5.5302
I (eV)	6.6767	6.6388	6.9775	6.8164	6.7786
A (eV)	− 0.255	− 0.221	0.6559	− 0.4345	1.2483
χ (eV)	3.2108	3.2089	3.8167	3.1909	4.0134
η (eV)	3.4658	3.4299	3.1608	3.6254	2.7651
σ (eV^{-1})	0.2885	0.2915	0.3163	0.2758	0.6316
ΔN	0.2321	0.2348	0.1587	0.2246	0.1458
$\Delta E_{back\text{-}donation}$	− 0.8664	− 0.8574	− 0.7902	− 0.9063	− 0.6912

As shown in Table 8, the E_{HOMO} values of the inhibitors studied decrease in order: β-pinene < terpene-4-ol < pulegone < eucalyptol < camphor, indicating that their capacity to transfer electrons to the MS interface increases by: β-pinene > terpene-4-ol > pulegone > eucalyptol > camphor. The capacity of an inhibitory molecule in interacting with the steel's surface can also be evaluated by exploring the energy gap (ΔE); the difference between E_{LUMO} and E_{HOMO}. The inhibitor's reactivity toward metallic surface increases with the ΔE decreases [68]. The ΔE values summarized in the table are as follows: eucalyptol > terpene-4-ol > β-pinene > camphor > pulegone, demonstrating an increase in the examined compounds' reactivity toward the metallic surface in the order: eucalyptol < terpene-4-ol < β-pinene < camphor < pulegone.

Electronegativity (χ) is an important concept which demonstrates the molecule's ability to gather electrons from its electronic surrounding. This chemical parameter may also provide details on the inhibitor's reaction with the metallic surface. The table shows that the χ of the investigated chemicals increases in the sequence: eucalyptol < β-pinene < terpene-4-ol < camphor < pulegone. Global hardness (η) and its reciprocal global softness (σ) are two chemical concepts that are extremely useful for understanding the reactivity between inhibitor and the surface of the bulk metal. η is considered as the electron cloud's resistivity to polarization or chemical species deformity during the chemical reaction. It is anticipated that inhibition performance will increase at higher molecular σ and lower molecular η. Based on the outcomes reported in the table, η values increase in the following order: pulegone < camphor < β-pinene < terpene-4-ol < eucalyptol, which means that the σ values increase in the opposite direction: eucalyptol < terpene-4-ol < β-pinene < camphor < pulegone.

3.11.2 MC Simulation

MC simulations make it feasible to forecast the actions of inhibitor compounds on metal surfaces. The found adsorption configuration and positions of selected organic compounds were indicated in Fig. 15.

Figure 15 shows the adsorption energies for the compounds. The E_{ads} result from the energy produced during the adhesion of the relaxed components to the substrate. E_{ads} is the result of adding the rigid distortion and adsorption energies of the adsorbent component. The evidence of elevated negative adsorption energy values reveals an increased interaction between Fe(110) and an inhibiting molecule. According to these results, the order of inhibitory potency of selected compounds is as follows: terpene-4-ol > pulegone > camphor > eucalyptol > β-pinene (Fig. 15).

3.11.3 MD Simulation

Molecular dynamics simulations were performed to examine sorption comportment of inhibitors β-pinene, camphor, eucalyptol, terpene-4-ol, and pulegone on the Fe(110). Interaction of the inhibitory compounds with the iron surface Fig. 16 exhibits the best adsorption patterns for various substances from Fig. 17, it is clear that the five molecules under investigation (β-pinene, camphor, eucalyptol, terpene-4-ol, and pulegone) are almost plane-oriented adsorbed to the surface of the steel. According to the quantum chemical study, the oxygen atoms in the examined compounds can transfer electrons to the vacant "d" iron orbital to form coordinating bonds, whereas orbitals π can accept electrons from the iron orbit "d" to form coordinating bonds.

The binding length of the Fe to the α-pinene, β-pinene, camphor, eucalyptol, and pulegone molecules was calculated using the RDF analysis. The various types of formed links were identified through the calculation of the bond length values. It is also revealed that the values of metal–oxygen bonds describe the type of adsorptive activity that takes place over the metal [1]. Chemisorption is considered to be occurring when the RDF peak is observed between 1 and 3.5 Å, while over this value, bond length shows the physisorption behavior.

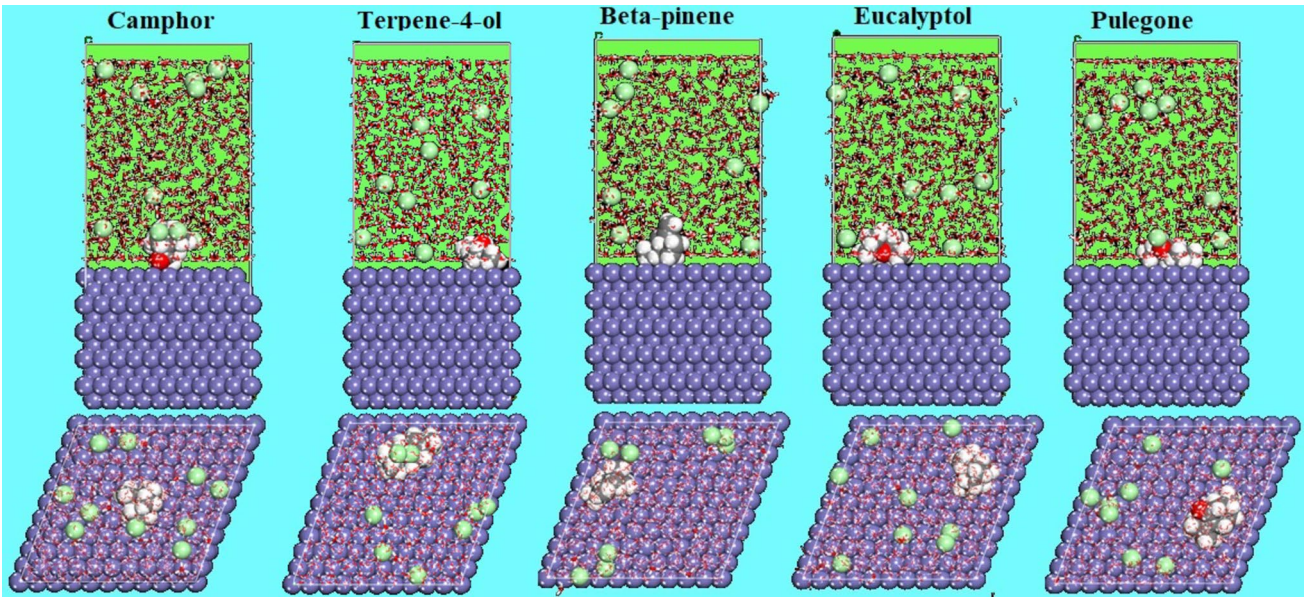

Fig. 15 MC simulation results: setups and adsorption positions of β-pinene, camphor, eucalyptol, terpene-4-ol, and pulegone molecules on the Fe(110) surface

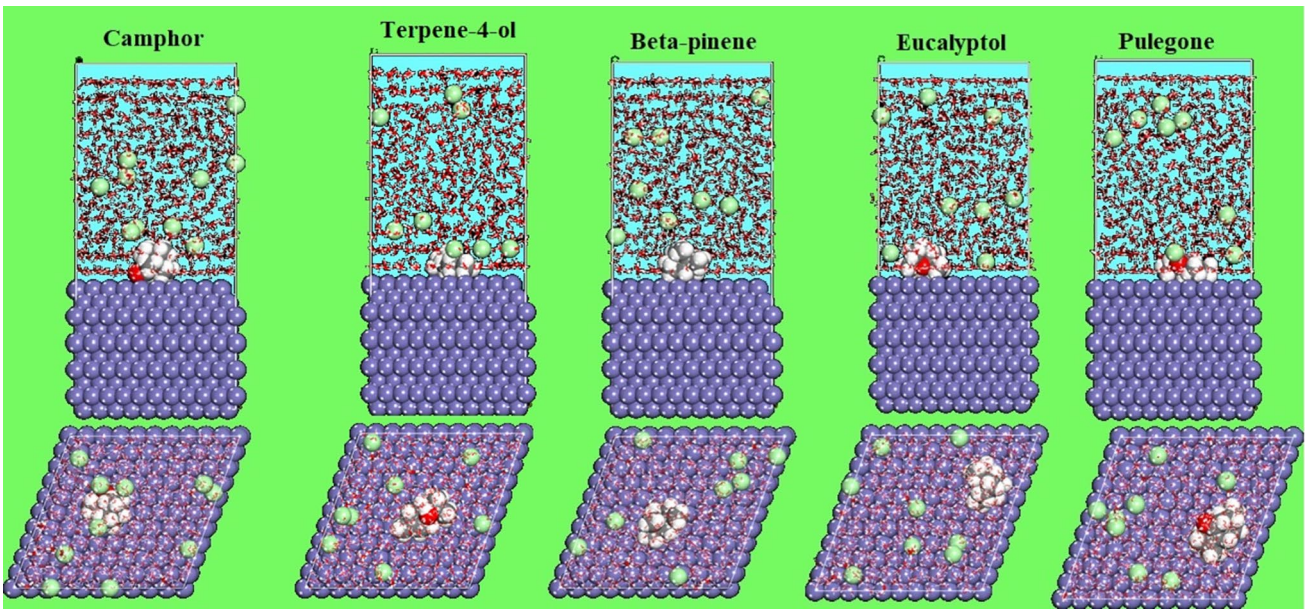

Fig. 16 Results of MD simulations: adsorption configurations and locations of β-pinene, camphor, eucalyptol, terpene-4-ol, and pulegone molecules on the Fe(110) surface

As indicated, the closeness of the phytochemicals atoms on the metal surface (Fig. 18) confirms the presence of a relatively significant interaction between the inhibitors and the metallic substrate. This sustains the inhibitor's reflective inhibitory performance [2, 3].

3.12 Adsorption Process

The inhibitor under investigation adheres to the metal surface by displacing H_2O molecule that has initially been adsorbed; this process can be described by the expression bellow:

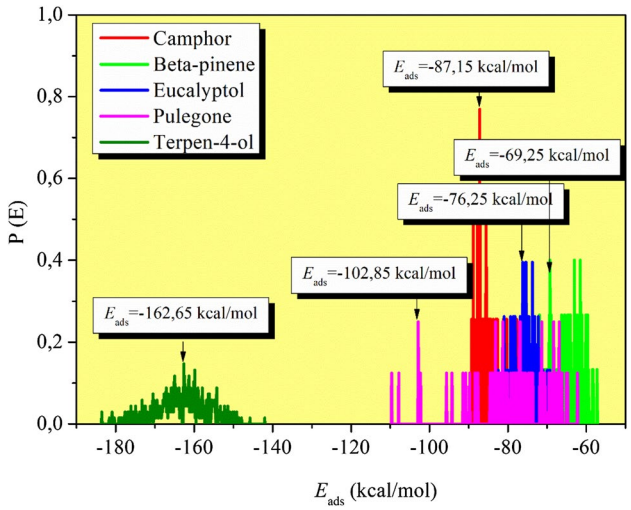

Fig. 17 Distribution of the E_{ads} for the major molecules of RAO oil onto the Fe(110) surface via MC simulations

$$In h_{(sol)} + nH_2O_{(ads)} \rightarrow In h_{(ads)} + nH_2O_{(sol)}$$

Inhibitor in solution is referred to $In h_{(sol)}$, $In h_{(ads)}$ is the inhibitor adhered to the MS surface, while $H_2O_{(sol)}$ is water molecules existing in solution and $H_2O_{(ads)}$ is the atoms that were initially engraved on the steel's surface, whereas n is the number of molecules of water (H_2O). that have been replaced by the inhibitor. The protonated form of *A. absinthium* oil molecules can interact electrostatically (physisorption) and via a synergistic interaction involving the pre-adhered Cl^-, also interactions can occur between heteroatoms and aromatic rings lone pair electron and those in d-orbital of Fe atoms (chemisorption) [69] (Fig. 19). Additional negative charges that accumulate on the surface of iron might be donated to essential oil molecular π* anti-bonding (retro-donation) [70]. Based on the analysis and assumptions provided above, we can conclude that our oil adsorbs physically and chemically on the iron and blocks the engaged sites thus mitigating corrosion in the aggressive medium [71].

3.13 Comparison of Inhibitive Power with Ozther Essential Oils

Literature study shows that essential oils exhibit great anti-corrosive properties, Table 9 shows the inhibitive power of some essential oils.

Due to their non-toxic effect, green plants exhibit biological and anti-corrosive proprieties, in this regard, plant extracts prove more interest than commercial inhibitors, it is crucial to recognize that all parts of plant (roots, stem, fruit, peel, seed) contribute to the inhibition of corrosion, however leaves have shown great richness in phytochemicals [75]. It is evident that the protection of the metal or allow in the acidic medium provided by these active chemicals results from their adsorption and development of a barrier that blocks the active sites For all plants extracted oil, the inhibitive power occurs by a synergic effect that includes constituents present in the oil [76]. By comparing table results we can notice that the *A. absinthium* oil is a powerful inhibitor against corrosion in HCl medium,

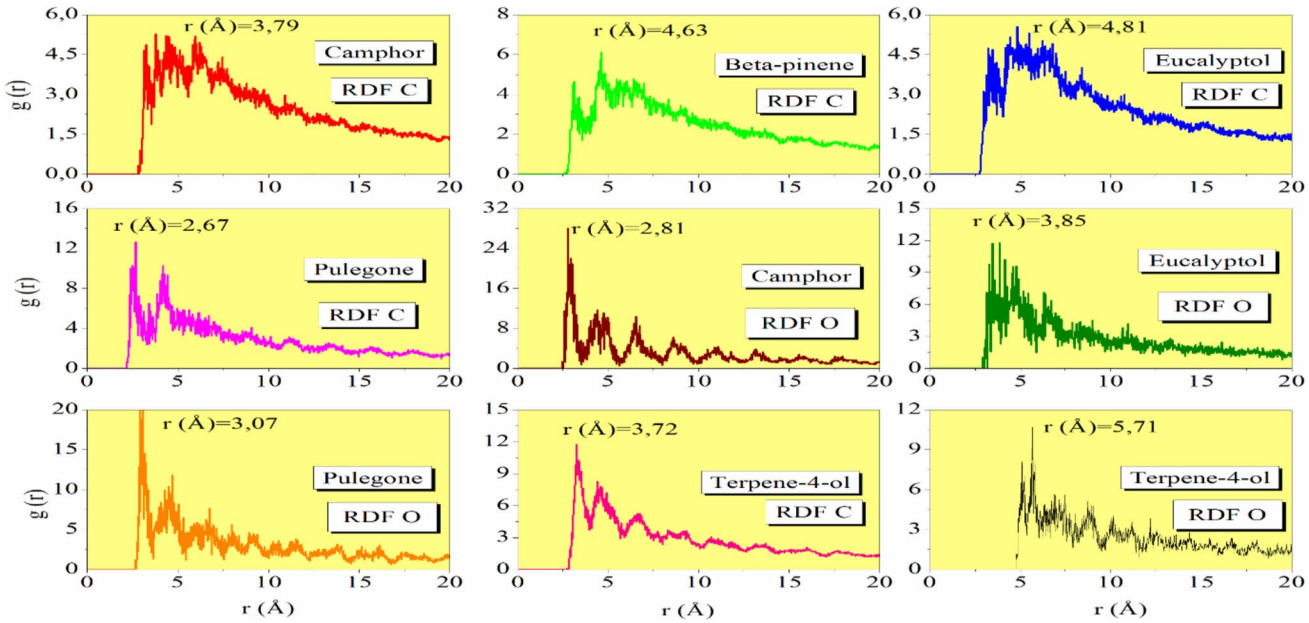

Fig. 18 RDF of the C and O atoms for the major molecules present in RAO oil, obtained via MD

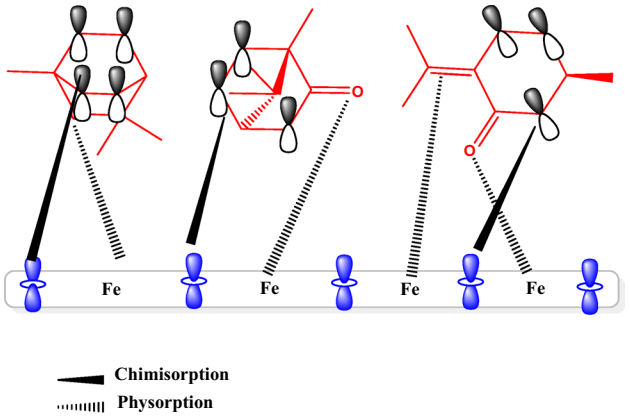

Fig. 19 The proposed mechanism of inhibition by RAO

Table 9 Comparative table of the performance of various essential oils

Essential oils	C_{inh} (g/l)	Medium	η (%)	References
Cinnamon	0.5	1 M HCl	84.64	[72]
Asteriscus graveolens	0.3	1 M HCl	74.27	[73]
Pulicaria incisa	0.3	1 M HCl	82.05	[73]
Schinus molle	2	1 M HCl	70	[74]
Pennyroyal mint	2.76	1 M HCl	80	[18]
Seed of the red pepper	2	1 M HCl	92.32	[19]
Calamintha	1.5	1 M HCl	87.57	[17]
A. absinthium	2	1 M HCl	92.60	In this work

even at low concentration 2 g/l the RAO oil showed the best inhibitory efficiency.

4 Conclusion

As a result of this investigation, we can conclude that *A. absinthium* oil can be employed for MS in HCl media as a powerful corrosion inhibitor. This oil has an exceptionally potent inhibitory power. PDP results reveal that the essential oil is described as an inhibitor of mixed type, it has an impact on both the cathodic and anodic reactions, and Tafel law is validated. Also, EIS findings show that the increase of the organic molecule concentration decreases the capacitance of the double layer and the oil's sorption to the surface of the steel impedes the charge transfer. On the other hand, WS reveals that adding oil to the acidic solution lowers the rate of corrosion in deed the η_w(%) reached 91.63% at the optimum concentration 2 g/l which is closely correlated with the outcomes obtained by the PDP (92.60%) and the EIS (91.85%) techniques. Thus, excellent agreement is seen between the potentiodynamic polarization, gravimetric, and EIS measurements. The immersion time study indicates that a progressive creation of a protective layer on the substrate's surface, while the impact of temperature demonstrates that the IE (%) decreases steadily with augmenting temperature, and its adsorption conforms to the isotherm model of Langmuir. The surface analysis techniques confirm the existence of a barrier protecting the metal. Finally, the quantum investigation proves the validity of the experimental study.

Author Contributions S.L: Investigation, conceptualization, methodology and editing, writing—original draft, software and visualization. W.D: Software, reviewing and editing, software and visualization. A.E: Conceptualization, methodology, writing—original draft. O.D: Formal analysis. H.K: Software, data curation. F.B: Formal analysis. A.B: Methodology, writing—original draft. A.B: Investigation, conceptualization. W.B: Methodology, reviewing and editing. A.Z: Software, reviewing and editing. A.L: Editing and review. All authors have read and agreed to the published version of the manuscript.

Funding This research received no external funding.

Data Availability Data will be made available on request.

Declarations

Competing interests Authors declare no competing financial interests.

References

1. Benhiba F, Hsissou R, Benzekri Z, Belghiti M, Lamhamdi A, Bellaouchou A et al (2020) Nitro substituent effect on the electronic behavior and inhibitory performance of two quinoxaline derivatives in relation to the corrosion of mild steel in 1 M HCl. J Mol Liq 312:113367
2. Lgaz H, Bhat KS, Salghi R, Jodeh S, Algarra M, Hammouti B et al (2017) Insights into corrosion inhibition behavior of three chalcone derivatives for mild steel in hydrochloric acid solution. J Mol Liq 238:71–83
3. Shahmoradi A, Ranjbarghanei M, Javidparvar A, Guo L, Berdimurodov E, Ramezanzadeh B (2021) Theoretical and surface/electrochemical investigations of walnut fruit green husk extract as effective inhibitor for mild-steel corrosion in 1 M HCl electrolyte. J Mol Liq 338:116550
4. Ansari K, Ramkumar S, Nalini D, Quraishi M (2016) Studies on adsorption and corrosion inhibitive properties of quinoline derivatives on N80 steel in 15% hydrochloric acid. Cogent Chem 2:1145032
5. Dutta A, Saha SK, Adhikari U, Banerjee P, Sukul D (2017) Effect of substitution on corrosion inhibition properties of 2-(substituted phenyl) benzimidazole derivatives on mild steel in 1 M HCl solution: a combined experimental and theoretical approach. Corros Sci 123:256–266
6. Bentiss F, Traisnel M, Lagrenee M (2000) The substituted 1, 3, 4-oxadiazoles: a new class of corrosion inhibitors of mild steel in acidic media. Corros Sci 42:127–146
7. Verma DK, Kazi M, Alqahtani MS, Syed R, Berdimurodov E, Kaya S et al (2021) N–hydroxybenzothioamide derivatives as green and efficient corrosion inhibitors for mild steel: experimental, DFT and MC simulation approach. J Mol Struct 1241:130648
8. Fouda A, Abdel-Wahed H, Atia M, El-Hossiany A (2023) Novel porphyrin derivatives as corrosion inhibitors for stainless steel 304 in acidic

environment: synthesis, electrochemical and quantum calculation studies. Sci Rep 13:17593
9. Khaled MA, Ismail MA, El-Hossiany AA, Fouda AE-AS (2021) Novel pyrimidine-bichalcophene derivatives as corrosion inhibitors for copper in 1 M nitric acid solution. RSC Adv 11:25314–25333
10. Hossain S, Razzak S, Hossain M (2020) Application of essential oils as green corrosion inhibitors. Arab J Sci Eng 45:7137–7159
11. Al Jahdaly BA (2023) Rosmarinus officinalis extract as eco-friendly corrosion inhibitor for copper in 1 M nitric acid solution: experimental and theoretical studies. Arab J Chem 16:104411
12. Miralrio A, EspinozaVázquez A (2020) Plant extracts as green corrosion inhibitors for different metal surfaces and corrosive media: a review. Processes 8:942
13. Salleh SZ, Yusoff AH, Zakaria SK, Taib MAA, Seman AA, Masri MN et al (2021) Plant extracts as green corrosion inhibitor for ferrous metal alloys: a review. J Clean Prod 304:127030
14. Motawea M, El-Hossiany A, Fouda A (2019) Corrosion control of copper in nitric acid solution using *Chenopodium* extract. Int J Electrochem Sci 14:1372–1387
15. Chetouani A, Hammouti B, Benkaddour M (2004) Corrosion inhibition of iron in hydrochloric acid solution by jojoba oil. Pigm Resin Technol 33:26–31
16. Chaieb E, Bouyanzer A, Hammouti B, Benkaddour M, Berrabah M (2004) Corrosion inhibition of steel in hydrochloric acid solution by Rosemary oil. Trans Soc Adv Electrochem Sci Technol 39:58
17. El Aatiaoui A, Daoudi W, El Badri A, Salhi A, El Massaoudi M, El Boutaybi A et al (2022) Anticorrosive potential of essential oil extracted from the leaves of Calamintha plant for mild steel in 1 M HCl medium. J Adhes Sci Technol 37(7):1191–1214
18. Bouyanzer A, Hammouti B, Majidi L (2006) *Pennyroyal* oil from *Mentha pulegium* as corrosion inhibitor for steel in 1 M HCl. Mater Lett 60:2840–2843
19. Kurniawan F, Madurani KA (2015) Electrochemical and optical microscopy study of red pepper seed oil corrosion inhibition by self-assembled monolayers (SAM) on 304 SS. Prog Org Coat 88:256–262
20. Loto RT, Okorie E, Olukeye T (2019) Synergistic combination effect of clove essential oil extract with basil and atlas cedar oil on the corrosion inhibition of low carbon steel. S Afr J Chem Eng 30:28–41
21. Juteau F, Jerkovic I, Masotti V, Milos M, Mastelic J, Bessière J-M et al (2003) Composition and antimicrobial activity of the essential oil of *Artemisia absinthium* from Croatia and France. Planta Med 69:158–161
22. Chen S, Zhu B, Liang X (2020) Corrosion inhibition performance of coconut leaf extract as a green corrosion inhibitor for X65 steel in hydrochloric acid solution. Int J Electrochem Sci 15:1
23. El Ouadi Y, Lamsayah M, Bendaif H, Benhiba F, Touzani R, Warad I et al (2021) Electrochemical and theoretical considerations for interfacial adsorption of novel long chain acid pyrazole for mild steel conservation in 1 M HCl medium. Chem Data Collect 31:100638
24. Mourya P, Singh P, Tewari A, Rastogi R, Singh M (2015) Relationship between structure and inhibition behaviour of quinolinium salts for mild steel corrosion: experimental and theoretical approach. Corros Sci 95:71–87
25. Dagdag O, Safi Z, Hsissou R, Erramli H, El Bouchti M, Wazzan N et al (2019) Epoxy pre-polymers as new and effective materials for corrosion inhibition of carbon steel in acidic medium: Computational and experimental studies. Sci Rep 9:1–14
26. Hsissou R, Dagdag O, Abbout S, Benhiba F, Berradi M, ElBouchti M et al (2019) Novel derivative epoxy resin TGETET as a corrosion inhibition of E24 carbon steel in 1.0 M HCl solution. Experimental and computational (DFT and MD simulations) methods. J Mol Liq 284:182–192
27. Dagdag O, Berisha A, Safi Z, Hamed O, Jodeh S, Verma C et al (2020) DGEBA-polyaminoamide as effective anti-corrosive material for 15CDV6 steel in NaCl medium: computational and experimental studies. J Appl Polym Sci 137:48402
28. Dagdag O, Hsissou R, El Harfi A, Berisha A, Safi Z, Verma C et al (2020) Fabrication of polymer based epoxy resin as effective anti-corrosive coating for steel: computational modeling reinforced experimental studies. Surf Interfaces 18:100454
29. Dagdag O, Hsissou R, Berisha A, Erramli H, Hamed O, Jodeh S et al (2019) Polymeric-based epoxy cured with a polyaminoamide as an anticorrosive coating for aluminum 2024–T3 surface: experimental studies supported by computational modeling. J Bio- Tribo-Corros 5:1–13
30. El Faydy M, Benhiba F, Berisha A, Kerroum Y, Jama C, Lakhrissi B et al (2020) An experimental-coupled empirical investigation on the corrosion inhibitory action of 7-alkyl-8-Hydroxyquinolines on C35E steel in HCl electrolyte. J Mol Liq 317:113973
31. Dagdag O, Hsissou R, El Harfi A, Safi Z, Berisha A, Verma C et al (2020) Epoxy resins and their zinc composites as novel anti-corrosive materials for copper in 3% sodium chloride solution: experimental and computational studies. J Mol Liq 315:113757
32. Sharopov FS, Sulaimonova VA, Setzer WN (2012) Composition of the Essential oil of *Artemisia absinthium* from Tajikistan. Rec Nat Prod 6(2):127–134
33. Ech-chihbi E, Nahlé A, Salim R, Oudda H, El Hajjaji F, El Kalai F et al (2019) An investigation into quantum chemistry and experimental evaluation of imidazopyridine derivatives as corrosion inhibitors for C-steel in acidic media. J Bio Tribo-Corros 5:1–18
34. Chung I-M, Malathy R, Priyadharshini R, Hemapriya V, Kim S-H, Prabakaran M (2020) Inhibition of mild steel corrosion using *Magnolia kobus* extract in sulphuric acid medium. Mater Today Commun 25:101687
35. Madu J, Ifeakachukwu C, Okorodudu U, Adams F, Joseph I (2019) Corrosion inhibition efficiency of *Terminalia catappa* leaves extracts on stainless steel in hydrochloric acid. J Phys Conf Ser 1378:022092
36. Younis R, Hassan HM, Mansour R, El-desoky A (2015) Corrosion inhibition of *Carapichea ipecacuanha* extract (CIE) on copper in 1 M HNO_3 solution. Int J Sci Eng Res 6:761–770
37. Fouda A, Mohamed A, Khalid M (2016) *Trigonella stellate* extract as corrosion inhibitor for copper in 1 M nitric acid solution. J Chem Pharm Res 8:86–98
38. Fouda AEAES, Ahmed AEMM, El-Darier SM, Badr SE (2021) *Fagonia arabica* extract as a safe-environment green corrosion inhibitor for Cu in HNO_3 solution. J Chin Chem Soc 68:1445–1455
39. Fouda A, Shalabi K, Idress A (2015) *Ceratonia siliqua* extract as a green corrosion inhibitor for copper and brass in nitric acid solutions. Green Chem Lett Rev 8:17–29
40. Fouda A, Abdallah Y, Elawady G, Ahmed R (2014) *Zygophllum coccineum* L. extract as green corrosion inhibitor for copper in 1 M HNO_3 solutions. Int J 2:517–531
41. Al-Nami S, Fouda AE-AS (2020) Corrosion inhibition effect and adsorption activities of methanolic myrrh extract for Cu in 2 M HNO_3. Int J Electrochem Sci 15:1187–1205
42. Sharma SK, Mudhoo A, Jain G, Sharma J (2010) Corrosion inhibition and adsorption properties of *Azadirachta indica* mature leaves extract as green inhibitor for mild steel in HNO_3. Green Chem Lett Rev 3:7–15
43. Salim R, Ech-chihbi E, Oudda H, Aoufir Y, El-Hajjaji F, Elaatiaoui A et al (2016) The inhibition effect of imidazopyridine derivatives on C38 steel in hydrochloric acid solution. Der Pharma Chem 8:200–213
44. Dawood M, Alasady Z, Abdulazeez M, Ahmed D, Sulaiman G, Kadhum A et al (2021) The corrosion inhibition effect of a pyridine derivative for low carbon steel in 1 M HCl medium: complemented with antibacterial studies. Int J Corros Scale Inhib 10:1766
45. Hajjaji FE, Salim R, Ech-chihbi E, Titi A, Messali M, Kaya S et al (2021) New imidazolium ionic liquids as ecofriendly corrosion inhibitors for mild steel in hydrochloric acid (1 M): experimental and theoretical approach. J Taiwan Inst Chem Eng 123:346–362

46. Abd El-Maksoud S, Fouda A (2005) Some pyridine derivatives as corrosion inhibitors for carbon steel in acidic medium. Mater Chem Phys 93:84–90
47. Mert BD, Yüce AO, Kardaş G, Yazıcı B (2014) Inhibition effect of 2-amino-4-methylpyridine on mild steel corrosion: experimental and theoretical investigation. Corros Sci 85:287–295
48. Yıldız R, Döner A, Doğan T, Dehri İ (2014) Experimental studies of 2-pyridinecarbonitrile as corrosion inhibitor for mild steel in hydrochloric acid solution. Corros Sci 82:125–132
49. El-Hajjaji F, Messali M, de Yuso MM, Rodríguez-Castellón E, Almutairi S, Bandosz TJ et al (2019) Effect of 1-(3-phenoxypropyl) pyridazin-1-ium bromide on steel corrosion inhibition in acidic medium. J Colloid Interface Sci 541:418–424
50. Abdel-Gaber A, Rahal H, Beqai F (2020) Eucalyptus leaf extract as a eco-friendly corrosion inhibitor for mild steel in sulfuric and phosphoric acid solutions. Int J Ind Chem 11:123–132
51. Palaniappan N, Chowhan LR, Jothi S, Bosco IG, Cole IS (2017) Corrosion inhibition on mild steel by phosphonium salts in 1 M HNO_3 aqueous medium. Surf Interfaces 6:237–246
52. Jafari H, Akbarzade K, Danaee I (2019) Corrosion inhibition of carbon steel immersed in a 1 M HCl solution using benzothiazole derivatives. Arab J Chem 12:1387–1394
53. Shriver DF, Atkins PW, Langford CH (1994) Inorganic Chemistry, vol 790. Oxford University Press, Oxford, p 357
54. Hmamou DB, Salghi R, Zarrouk A, Zarrok H, Hammouti B, Al-Deyab S et al (2013) Electrochemical and gravimetric evaluation of 7-methyl-2-phenylimidazo [1, 2-α] pyridine of carbon steel corrosion in phosphoric acid solution. Int J Electrochem Sci 8:11526–11545
55. Abdel-Gaber A, Abd-El Nabey B, Sidahmed I, El-Zayady A, Saadawy M (2006) Effect of temperature on inhibitive action of *Damsissa* extract on the corrosion of steel in acidic media. Corrosion 62:293–299
56. Christov M, Popova A (2004) Adsorption characteristics of corrosion inhibitors from corrosion rate measurements. Corros Sci 46:1613–1620
57. Al-Amiery A, Shaker L (2020) Corrosion inhibition of mild steel using novel pyridine derivative in 1 M hydrochloric acid. Koroze a ochrana materiálu 64:59–64
58. Verma C, Rhee KY, Quraishi M, Ebenso EE (2020) Pyridine based N-heterocyclic compounds as aqueous phase corrosion inhibitors: a review. J Taiwan Inst Chem Eng 117:265–277
59. Verma C, Abdellattif MH, Alfantazi A, Quraishi M (2021) N-heterocycle compounds as aqueous phase corrosion inhibitors: a robust, effective and economic substitute. J Mol Liq 340:117211
60. Lukovits I, Kalman E, Palinkas G (1995) Nonlinear group-contribution models of corrosion inhibition. Corrosion 51:201–205
61. Daoudi W, El Ibrahimi B, Dagdag O, Berdimurodov E, Guo L, Ebenso EE et al (2023) New chlorophenyl-imidazole derivative as a novel corrosion inhibitor in the gas and oil industry. J Phys Chem Solids 179:111409
62. Haldhar R, Vanaraj R, Dagdag O, Berisha A, Kim S-C (2023) *Convolvulus microphyllus* extract as a green, effective, and affordable corrosion inhibitor: theoretical calculations and experimental studies. Coatings 13:860
63. Daoudi W, El Aatiaoui A, Dagdag O, Zaidi K, Haldhar R, Kim S-C et al (2023) Anti-corrosion coating formation by a biopolymeric extract of *Artemisia herba-alba* plant: experimental and theoretical investigations. Coatings 13:611
64. Ihamdane R, Tiskar M, Outemsaa B, Zelmat L, Dagdag O, Berisha A et al (2023) Essential oil of *Origanum vulgare* as a green corrosion inhibitor for carbon steel in acidic medium. Arab J Sci Eng 48:7685–7701
65. Daoudi W, Azzouzi M, Dagdag O, El Boutaybi A, Berisha A, Ebenso EE et al (2023) Synthesis, characterization, and corrosion inhibition activity of new imidazo [1.2-a] pyridine chalcones. Mater Sci Eng B 290:116287
66. Ganjoo R, Sharma S, Sharma PK, Dagdag O, Berisha A, Ebenso EE et al (2023) Coco monoethanolamide surfactant as a sustainable corrosion inhibitor for mild steel: theoretical and experimental investigations. Molecules 28:1581
67. Iroha NB, Anadebe VC, Maduelosi NJ, Nnanna LA, Isaiah LC, Dagdag O et al (2023) Linagliptin drug molecule as corrosion inhibitor for mild steel in 1 M HCl solution: electrochemical, SEM/XPS, DFT and MC/MD simulation approach. Colloids Surf A 660:130885
68. Zaidi K, Aouniti A, Merimi C, Daoudi W, Dagdag O, Berisha A et al (2023) Comparative study of inhibitory efficacy of methionine and its derivatives in acidic medium by mild steel. Moroccan J Chem 11(2):411–433
69. Adejo S, Ekwenchib M, Gbertyoa J, Menengea T, Ogbodoc J (2014) Determination of adsorption Isotherm model best fit for methanol leaf extract of *Securinega virosa* as corrosion inhibitor for corrosion of mild steel in HCl. J Adv Chem 10(5):2737–2742
70. Mahmoud ME, Amira MF, Seleim SM, Mohamed AK (2017) Adsorption isotherm models, kinetics study, and thermodynamic parameters of Ni (II) and Zn (II) removal from water using the LbL technique. J Chem Eng Data 62:839–850
71. Ituen E, Akaranta O, James A (2017) Evaluation of performance of corrosion inhibitors using adsorption isotherm models: an overview. Chem Sci Int J 18:1–34
72. Bouraoui MM, Chettouh S, Chouchane T, Khellaf N (2019) Inhibition efficiency of cinnamon oil as a green corrosion inhibitor. J Bio Tribo-Corros 5:1–9
73. Chaib F, Allali H, Benali O, Flamini G (2020) Corrosion inhibition effects of the essential oils of two Asteraceae plants from South Algeria. Int J Chem Biochem Sci 18:129–136
74. Mellak N, Ghali N, Messaoudi N, Benhelima A, Ferhat M, Addou A (2021) Study of corrosion inhibition properties of *Schinus molle* essential oil on carbon steel in HCl. Mater Corros 72:1270–1278
75. Kadhim A, Betti N, Al-Bahrani H, Al-Ghezi M, Gaaz T, Kadhum A et al (2021) A mini review on corrosion, inhibitors and mechanism types of mild steel inhibition in an acidic environment. Int J Corros Scale Inhib 10:861–884
76. Bensouda Z, Driouch M, Belakhmima R, Sfaira M, Touhami ME, Farah A (2018) *Thymus sahraouian* essential oil as corrosion ecofriendly inhibitor for mild steel in a molar hydrochloric acid solution. Port Electrochim Acta 36:339–364